

Lattice Metamaterials with Mesoscale Motifs: Exploration of Property Charts by Bayesian Optimization

Roman Kulagin,* Patrick Reiser, Kyril Truskovskiy, Arnd Koeppel, Yan Beygelzimer, Yuri Estrin, Pascal Friederich, and Peter Gumbsch

Through the current work, the usefulness of the concept of architected rod lattices based on unit cell motifs designed at mesoscale is demonstrated. Specifically, 2D triangular lattices with unit cells containing different numbers of rods are considered. Combinations of rods of two different types provide the lattices explored with a greater complexity and versatility. For mesocells with a large number of variable parameters, it is virtually impossible to calculate the entire set of the points mapping the material onto its property space, as the volume of calculations would be gigantic. The number of possible motifs increases exponentially with the number of rods. Herein, the lattice metamaterials with mesoscale motifs are investigated with the focus on their elastic properties by combining machine learning techniques (specifically, Bayesian optimization) with finite element computations. The proposed approach made it possible to construct property charts illustrating the evolution of the boundary of the elastic compliance tensor of lattice metamaterials with an increase in the number of rods of the mesocell when a full-factor experiment would not be possible.

properties.^[1–3] One of the subclasses of this kind of material is lattice (meta)materials. Classical lattice materials have a mesh-like structure generated by translation in space of an elementary cell that comprises several, most commonly identical, elements, such as thin bars or rods.^[4,5] It was found that materials with this type of inner architecture while having a low density, exhibit high values of stiffness, strength, and fracture toughness.^[4–6] Great expectations in this field are connected with nanoscale lattices.^[7,8]

Two principal directions can be followed to get to more versatile behavior. First, lattice-based metamaterials can, of course, be built from more complex unit cells. Buckling elements in the unit cell can effectively give a plastic response,^[9] chiral elements can show macroscopically chiral response,^[10] and gear-based lattice structures can change connectivity and allow extreme

adaptivity of elastic properties even in the built structure.^[11]

The second direction is to build lattice materials with a structure different from the classical one, which possesses new properties.^[12] For example, it was shown that irregular mesh

1. Introduction

Architectural materials at mesoscale open new opportunities for the design of materials with unique combinations of

R. Kulagin, P. Reiser, P. Friederich
Institute of Nanotechnology
Karlsruhe Institute of Technology
Hermann-von-Helmholtz-Platz 1, 76344 Eggenstein-Leopoldshafen,
Germany
E-mail: roman.kulagin@kit.edu

P. Reiser, P. Friederich
Institute of Theoretical Informatics
Karlsruhe Institute of Technology
Engler-Bunte-Ring 8, 76131 Karlsruhe, Germany

K. Truskovskiy
Borealis AI
Montreal QC H2S 3H1, Canada

A. Koeppel
Institute for Applied Materials (IAM-MMS)
Karlsruhe Institute of Technology
Straße am Forum 7, 76131 Karlsruhe, Germany

Y. Beygelzimer
Donetsk Institute for Physics and Engineering named after A.A. Galkin
National Academy of Sciences of Ukraine
Nauki Ave., 46, 03028 Kyiv, Ukraine

Y. Estrin
Department of Materials Science and Engineering
Monash University
22 Alliance Lane, Clayton 3800, Australia

Y. Estrin
Department of Mechanical Engineering
The University of Western Australia
Crawley 6009, Australia

P. Gumbsch
Institute for Applied Materials
Karlsruhe Institute of Technology
Straße am Forum 7, 76131 Karlsruhe, Germany

P. Gumbsch
Fraunhofer Institute for Mechanics of Materials IWM
Wöhlerstraße 11, 79108 Freiburg, Germany

 The ORCID identification number(s) for the author(s) of this article can be found under <https://doi.org/10.1002/adem.202300048>.

© 2023 The Authors. Advanced Engineering Materials published by Wiley-VCH GmbH. This is an open access article under the terms of the Creative Commons Attribution-NonCommercial License, which permits use, distribution and reproduction in any medium, provided the original work is properly cited and is not used for commercial purposes.

DOI: 10.1002/adem.202300048

structures offer broad possibilities in the design of materials with superior functional characteristics.^[13] These include insensitivity to crystal lattice defects, the efficacy of impact energy absorption, and redistribution of internal stresses. A recent article discusses materials with regular or irregular lattice structure assembled from specially designed building blocks, which exhibit a superior buckling resistance.^[14] A new strategy for the design of chiral materials based on the idea that their lattice consists of two types of unit cells rotating in opposite directions during deformation has been presented.^[15] The idea of designing a metamaterial with the desired structural properties based on a macroscopic periodic lattice composed of optimized microscopic unit cells has been proposed.^[16] In recent publications, lattice metamaterials with mesoscale motifs (LMMM) were introduced.^[3,17] They are characterized by a multiscale architecture with a regular lattice at the lowest length scale, which entails structural elements (rods, nodes) of more than one type. Thanks to this architecture, mesoscale patterns can form at a higher length scale. This enables radical changes in the properties of the overall lattice structure, inducing, for instance, tuneable anisotropy. The elastic compliance tensor can thus be controlled both by variation of the mesoscale architecture and by tuning the characteristics of the elements of the structure.

Because of a large number of possible variants of the mesostructure, the design of LMMMs poses a challenging problem. Indeed, if the elementary cell of the mesostructure contains n elements (rods, beams), each of which belonging to one of k possible types, then k^n variants of the mesh architecture are possible. Already for relatively modest values of $n = 50$, $k = 2$, a very large number of different patterns, $2^{50} \approx 10^{15}$, would exist. On the one hand, this suggests a broad range of possibilities of LMMM. On the other hand, this illustrates the difficulty with choosing the architecture variant that would ensure an optimum according to specified design criteria.

Lattice materials for which k and n are given contain a certain number of mesostructures corresponding to a set of points that represent their characteristics in the property space. Such a property space is multidimensional, and to simplify analysis and the practical use, its 2D projections are commonly used.^[17] In fact, they can be viewed as Ashby's material property charts, reflecting the ranges of variation of the properties of LMMMs. The experience with using such charts shows that they greatly facilitate the search for effective materials and their design.^[18] Recent studies in this area have generated a great deal of activity in materials design and discovery.^[19,20]

Building LMMM property charts with a large number n of structural elements in a mesocell is a difficult task, since the required volume of calculations grows with increasing n according to a power-law, k^n , where k is the number of different kinds of rods in the structure. This article aims to solve this formidable problem. It presents an approach to finding new points in the property space that represent an expansion of the mapping of this space onto the 2D property charts. We are proposing a tool for searching for an LMMM architecture whose properties form a limiting boundary on the corresponding property chart. The approach uses the Bayesian optimization method and is based on a relatively small number of calculations, which allows us to find the approximate shape of the LMMM property charts at a reasonable computational

cost. In addition, we have established the general patterns of evolution of LMMM property charts with an increase in the number of structural elements in a mesocell.

2. Limit Properties of LMMM Property Charts

We consider the limit properties of the LMMM property charts by considering the elastic compliance tensor. The region in the elastic compliance space Z populated by the set of points representing all possible LMMM with n structural elements in the mesoscale unit cell is denoted by Ω_n and its outer boundary is denoted by $\partial\Omega_n$. In this section, we demonstrate that for fixed properties of structural elements, an increase in n leads to a progressively denser filling of Ω_n with the representative points. Concurrently, its boundary $\partial\Omega_n$ expands, asymptotically approaching a limited surface $\partial\Omega$. This means that for $n \rightarrow \infty$, the limit region Ω with a boundary $\partial\Omega$ is formed.

To prove the posited statement, we consider, again without loss of generality, the case when an LMMM has structural elements of just two possible kinds, with the elastic moduli E_1 and E_2 . Let us introduce the following notation: G_n denoting the set of mesostructures with n rods within the elementary cell; $A_{i,n}$ denoting the i -th mesostructure from within this set (in the case of two kinds of rods, i is in the range $1 \leq i \leq 2^n$); and Z denoting the 6D space of the elastic compliance, with $Z(A_{i,n})$ representing a point in the latter space which corresponds to an LMMM with the mesostructure $A_{i,n}$.

For a fixed value of n , the points with $1 \leq i \leq 2^n$ populate the region Ω_n , with the boundary $\partial\Omega_n$, in the Z space. These are examples of material property charts, which provide a visual representation of the elastic characteristics of the LMMM.^[17]

We now posit that there exists a limit surface toward the outer boundaries of the sets $Z(A_{i,n})$ tend when $n \rightarrow \infty$. To that end, we consider a geometric sequence of sets G_n , in which each value of n doubles that of the previous one (for example, $n = 3, 6, 12, 24, \dots$). Assuming $n_2 > n_1$, a special case of a mesoscale cell with n_2 rods is its filling with $\frac{n_2}{n_1}$ identical mesoscale cells with n_1 rods. It follows that the set G_{n_2} contains all elements of the set G_{n_1} , which means that the region Ω_{n_2} includes the region Ω_{n_1} . Let D_n be the size of the region Ω_n in an arbitrary direction of the space Z . From the previous statement, it follows that with growing n , the quantities D_n form a monotone growing sequence. Compliance moduli are limited in magnitude for physical reasons because unlimited compliance would mean non-zero deformation under the action of zero load. According to the Bolzano–Weierstrass theorem, any bounded monotone sequence has a limit.^[21] It follows that all regions Ω_n are inserted within some limit region Ω , the boundaries $\partial\Omega_n$ tending to $\partial\Omega$ asymptotically when $n \rightarrow \infty$. The limit boundary $\partial\Omega$ is the boundary in the elastic compliance space Z for LMMM for the considered sequence n .

Let us now take a mesoscale cell ("mesocell" for short) that contains an arbitrary number m of rods, with m not belonging to the sequence n considered previously. For $n \gg m$, i.e., for the case when a cell with n rods contains many cells with m rods, a mesocell with n rods can be represented as an integer number $\lfloor \frac{n}{m} \rfloor$ of mesocells with m rods and a residual structure with $\{n\} = n - \lfloor \frac{n}{m} \rfloor m$ rods. It is reasonable to postulate that the effect of the residual

structure on the elastic moduli of the material can be neglected for a sufficiently small ratio $\frac{\{n\}}{n}$. Consequently, for any m , one can find such a large value of n from the geometric sequence considered previously that the elastic compliances of the material with a mesocell with m rods will practically coincide with those of the material with an n -rod mesocell. In other words, for the case of two types of rods, LMMM with any number of rods in the mesocell will have the same limit boundary of the elastic compliances in the Z space.

Now we consider a further property of the LMMM structures, namely an increase in the density with which the representative points populate the region Ω with an increase in the number of the structural elements in a mesocell. Indeed, to each mesoscale structure with a unit cell composed of n structural elements, one can ascribe a binary number (c_1, c_2, \dots, c_n) , where c_i can be 0 or 1, depending on the type of the element, a or b , located in the corresponding position. This means that for $n \rightarrow \infty$ all possible mesoscale structures form a countable set. It is mapped onto a limited region of the elastic compliance space by means of the function $Z(A_{i,n})$. In this way, for $n \rightarrow \infty$, a countable set of points $Z(A_{i,n})$ is formed in a bounded volume of the Z space. It is known that a countable set is dense in the space of real numbers, i.e., any point in the Z space can be represented by the points $Z(A_{i,n})$ with a desired degree of precision.^[22] This reasoning proves the previous statement.

3. Methodology of LMMM Property Chart Calculations

To elucidate the features of LMMM Property Chart limits, we consider the case when all nodes of a rod lattice are rigid. Rod elements of just two kinds—identical in terms of their geometry but different in stiffness—are admitted. The elastic modulus of the rods of the first and second kinds are set at 100 and 10 MPa, respectively. All rod elements are treated as Bernoulli beams 10 mm in length with a square-shaped cross-section 1 mm × 1 mm in size. Five LMMM arrays with

mesoscale unit cells composed of 3, 12, 27, 48, and 75-rod elements were analyzed. They generated, respectively, $2^3 = 8$, $2^{12} = 4,096$, $2^{27} \approx 10^8$, $2^{48} \approx 10^{14}$, and $2^{75} \approx 10^{23}$ possible LMMMs. **Figure 1** displays examples of patterns of mesocells, along with the corresponding structures at mesoscale.

The calculations are limited to small elastic deformations of 2D lattices within the linear elasticity theory. The components of the linear compliance tensor were calculated using the Representative volume element (RVE) approach.^[17] An RVE containing 10×10 mesocells was chosen. The volume of computations involved in this method is much greater than that required when homogenization with periodic boundary conditions is used. We opted for the former despite this computational cost because an RVE of a size much bigger than that of a mesocell enables accounting for possible nonuniformities at mesoscale, such as the presence of mesocells with different structure in the mesh or random defects in rod or node elements. Besides, the choice of a mesoscale motif is not unique, which can lead to different results when periodic boundary conditions are employed.^[23,24]

The ideated problem we are trying to solve in this manuscript is a high-dimensional (global) optimization problem with potentially nonsmooth surfaces. Such optimization problems can be addressed with various algorithms (e.g., gradient methods, genetic algorithms, etc.). However, all of these techniques require a large number of ground truth evaluations, which is not feasible computationally considering the humongous size of the search space (2^n). One could choose a way of replacing the ground truth evaluation with a trained surrogate model. Given the type of input we have here, graph neural networks or convolutional neural networks would be most suitable.^[25,26] However, optimization based on such a surrogate model would not be sufficient in our case, as the regions of interest (i.e., extremal properties) are populated very scarcely and are not covered by any randomly drawn initial dataset.^[27–29] Therefore, active learning approaches are required to make the most efficient use of the costly ground truth evaluations (i.e., simulations). Bayesian optimization can be seen as one

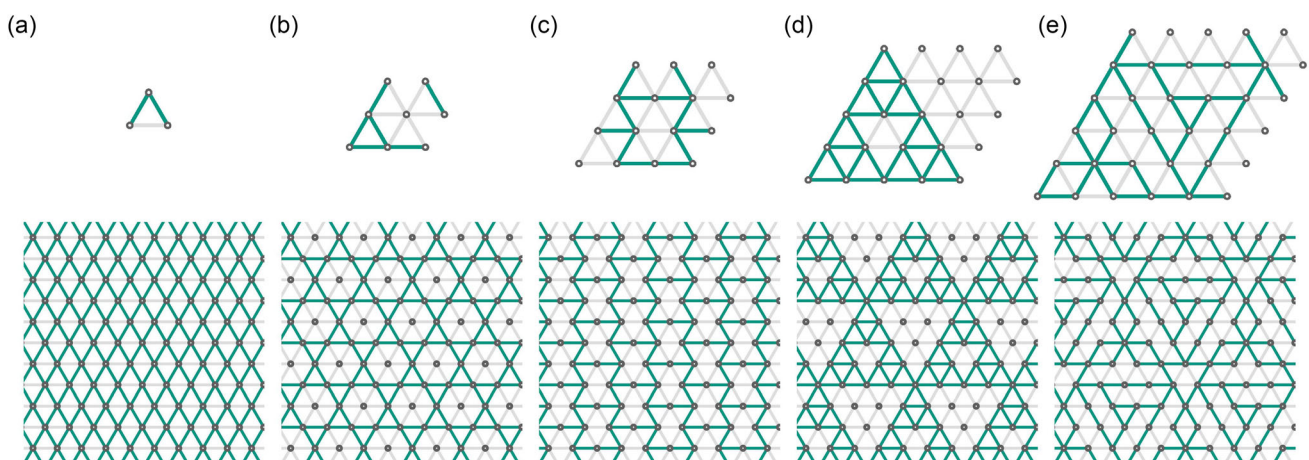


Figure 1. Examples of LMMM structures for mesocells with different numbers of independent rods: a) $n = 3$; b) $n = 12$; c) $n = 27$; d) $n = 48$; e) $n = 75$. The upper row shows the mesocell motifs, and the lower one shows the corresponding structures at mesoscale. The two different colors of the rods reflect the difference in their elastic moduli.

(highly efficient) approach to implementing active learning, where the surrogate model (in our case, a Gaussian process regression model) is updated iteratively to learn from ground truth evaluations in a data-efficient way. Given the size of the input space and the cost of ground truth evaluations, we found Bayesian optimization to be the most promising way of finding a large number of optima/extrema in a complex and high-dimensional space. For larger lattice sizes and potentially more complex lattice representations (e.g., grid representations), other approaches, e.g., a combination of active learning and deep learning surrogate models or inverse models (e.g., conditional generative models), might be the optimal choice.^[30]

For mesocells with 3 and 12 elements, full factorial simulations were conducted, in which the elastic compliance tensor was determined for all possible variants of mesocells. Because of the enormously large numbers of the variants of mesocells with 27, 48, and 75 elements, the contours of the LMMM property charts and the density of their filling were determined based on Bayesian optimization in the following form

$$\max_{Z_i, Z_j} \left(\alpha \frac{Z_i - \bar{Z}_i}{\hat{Z}_i} + \beta \frac{Z_j - \bar{Z}_j}{\hat{Z}_j} \right), \quad (1)$$

where α and β are the parameters of the optimization grid $[-1, -0.9, \dots, 0.9, 1] \times [-1, -0.9, \dots, 0.9, 1]$; \bar{Z} and \hat{Z} denote, respectively, the mean values and the amplitude of the components of the elastic compliance tensor of the LMMMs.^[31]

The 6D space of the elastic compliances has 15 independent projections. The following algorithm was applied for each of them. First, 2,000 random lattice patterns were generated. For them, the mean values (\bar{Z}_i, \bar{Z}_j) and the variations (\hat{Z}_i, \hat{Z}_j) for a given projection were determined. Then, for each combination of α and β considered, 400 iterations of the Bayesian optimization were carried out. For each iteration, the elastic properties were calculated using the finite element method. For each mesocell, more than 2.6 million mesoscale structures were included in the computations, see more details in **Table 1**.

4. Results

The results of the calculations of the evolution of the LMMM property charts with the number of structural elements in the mesoscale cells are shown in **Figure 2** on three exemplary

Table 1. Mesocell calculation parameters.

Number of independent rods in the mesocell	Number of possible motifs	Number of simulations	Fraction of the considered motifs among the total number of motifs [%]
3	8	8	100
12	4096	4096	100
27	1.34×10^8	2.64×10^8	2
48	2.81×10^{14}	2.64×10^8	9.4×10^{-7}
75	3.78×10^{22}	2.64×10^8	7.0×10^{-15}

projections. The complete set of all 15 planar projections of the 6D space of the elastic compliance tensor is shown in **Figure 3**.

The evolution of the population of the property space shown in **Figure 2** for three projections of the elastic compliance tensor is characteristic for all 15 projections. The projection on the (Z_{2222}, Z_{1111}) plane, **Figure 2a**, is interesting in that the smallest mesocell with just three elements yields a combination of the “extremal” components of the compliance tensor. That is to say, the points corresponding to this mesocell are situated on the perimeter of the limit region Ω . This region gets filled with the points representing materials with new properties as the number of the independent elements in the mesocell increases. A remarkable observation is that for these uniaxial compliances, the additional degrees of freedom introduced when the number of the elements in the mesocell is increased do not cause an expansion of the property chart. It is also surprising that even the simplest mesocell with just three independent rod elements gives rise to a mesoscale pattern which brings about properties substantially different from those predicted by the mixture rules. The projection on the (Z_{2222}, Z_{1122}) plane, **Figure 2b** reveals that the main effect of using mesocells with greater complexity consists in a higher density with which the representative points populate the property chart. Starting from $n = 27$, new areas emerge, which means that the property space is expanding in Z_{1122} direction. An example of cardinally new properties generated by using the unit cell with 27 elements is the structure presented previously in **Figure 1c**, which is a classical exemplar of an auxetic. In the projection on the (Z_{2222}, Z_{1112}) plane shown in **Figure 2c**, the effect of the complexity of the material architecture is expressed even more prominently. The properties of the rod lattice generated by the three-rod mesocell are practically identical with those following from the rule of mixtures. With an increase in the number of elements of the mesocell, the range of attainable properties expands.

The first characteristic type of the filling of the LMMM property charts corresponds to the components Z_{1111} , Z_{2222} , and Z_{1212} of the elastic compliance tensor. This can easily be rationalized as uniform lattices composed of elements with the elastic moduli E_1 and E_2 produce the limit properties for the mentioned components. Additional degrees of freedom enable filling the space between these limit points but do not allow going beyond them. At the same time, the observations made for LMMMs with small values of n do not provide grounds to conclude that mesocells with a larger number of elements, e.g., $n = 12$ or $n = 27$, are sufficient to provide the full coverage of the limit region Ω . Indeed, despite a good coverage of the property region in these projections, it is the specific architecture, rather than the properties of the rod material that determines the properties of the lattice. For the Z_{1122} component, which upon normalization represents the Poisson ratio, the influence of the lattice architecture is quite prominent. A record, in terms of the significance of the architecture, is held by the projections Z_{1112} and Z_{2212} , which expresses the chirality of the material. Several projections of these components reveal that with the increasing mesocell size, the property space expands in all directions.

The shape of the property regions within the LMMM property charts is another aspect of interest. Of course, the results obtained with the aid of Bayesian optimization do not guarantee

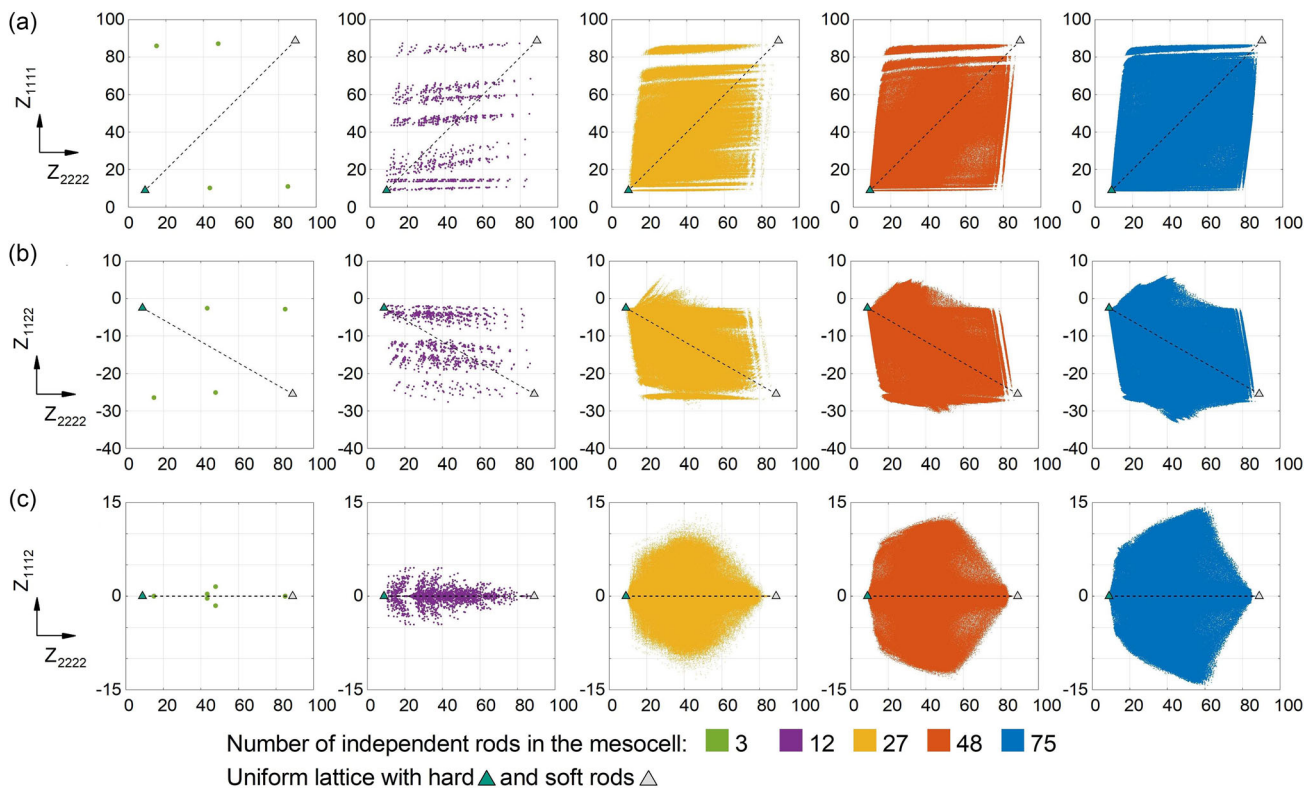


Figure 2. Examples of the evolution of the LMMM property charts with the number of the elements of mesoscale cells for projection on the a) (Z_{2222}, Z_{1111}) ; b) (Z_{2222}, Z_{1122}) ; c) (Z_{2222}, Z_{1112}) planes.

that for every mesocell considered the maximum property values corresponding to the limit boundary $\partial\Omega$ have been obtained, cf. Section 2. We note, however, that only some of the properties exhibit a potential for further expansion of the property charts. This needs to be considered in follow-up studies. For such follow-up studies, all investigated mesocell structures and the corresponding material properties are stored, managed, and published through the Kadi4Mat platform for research data management.^[32,33]

5. Discussion

The results obtained in this work demonstrate that architecturing the rod lattice structure at mesoscale does expand the realm of material properties. In each of the projections collated in Figure 2, two points are marked, which correspond to the lattices composed of one sort of the beams only. The straight segment connecting these points represents the possible material properties according to the rule of mixtures.^[34] Figure 3 shows that principally new properties not predictable by the rule of mixture can be obtained by means of architecturing rod lattice materials at mesoscale. It was also established that an increase in the number of the rod elements in the mesocell, the representative points of an LMMM structure fill the Z region, which concurrently expands in space, with ever-growing density and taking into account the sampling of the Bayesian optimization target. Despite the exponential growth in the number of motifs with

increasing n in the mesocell, not all motifs can be reproduced for the sequence $n = 27; 48; 75$ considered in the article. In some directions in Figure 3, a mesocell with a lower n can expand further than a mesocell with a larger n . It can be taken for granted that a motif can be completely copied when the mesocell is enlarged by an integer factor.

It is of interest to assess the growth of the LMMM property charts with the mesocell size. First, we have to specify what is considered as the area of a chart that maps sets of points rather than a continuum. For that, we introduce an interval Δ such that a change of the compliance within it can be neglected. It is natural to set $\Delta = \delta Z$, where Z is a characteristic value of the compliance and δ is a small parameter. We subdivide all projection planes into $\Delta \times \Delta$ squares. The area of a property chart will be defined as the quantity $S = N\Delta^2$, where N is the number of squares that contains at least one point from the set considered. Figure 4 displays the graphs of the $S(n)$ for all property charts in Figure 3 for $\delta = 10^{-3}$. They show that the most rapid growth of S with n occurs upon the transition from mesocells with $n = 12$ to those with $n = 27$. Subsequently, this growth is retarded, a tendency to saturation being recognizable in many projections. This is in accord with the observations made in Section 2.

Although the increase of the area of the property charts for large n is not very significant, investigating the evolution of the near-boundary zone is of interest, as it is this area where LMMM structures with record high characteristics may be found, cf. Section 4. In this regard, it is prudent to hypothesize about the

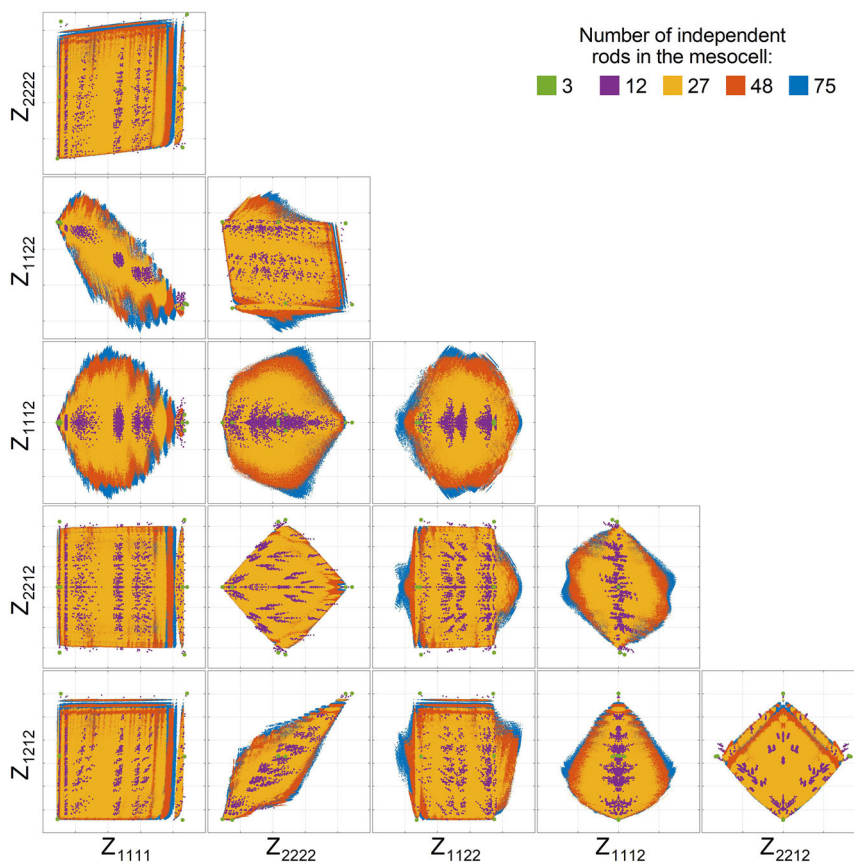


Figure 3. LMMM property charts for components of the elastic compliance tensor.

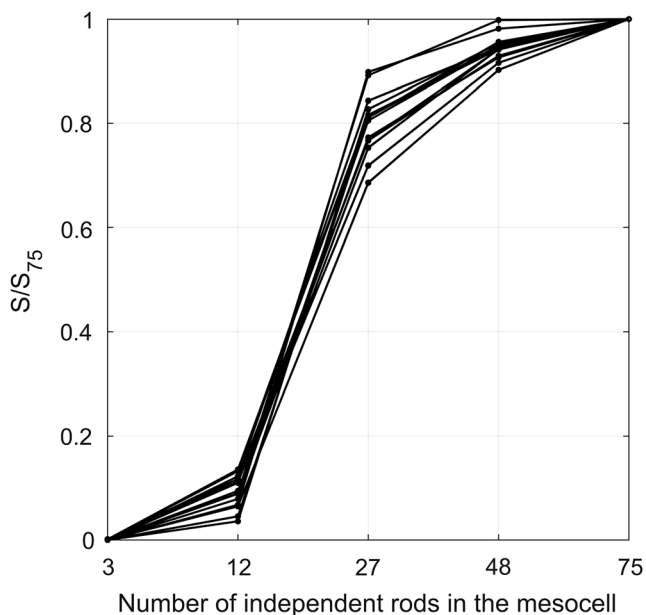


Figure 4. Evolution of the space-filling with the number of rod elements in the mesocell: The chart area S as a function of n for all charts in Figure 3.

characteristic size D of the limit region Ω . If all rod elements of a lattice material are of the same type, there exists just a single

representative point in the Z space corresponding to it. One can hypothesize that D is determined by the difference in the mechanical characteristics of the rod elements of the two possible types. Then, it follows from dimensional considerations that $D \approx |E_1^{-1} - E_2^{-1}|$ holds. We stress that this is a plausible evaluation, not a real quantitative estimate of D . Moreover, it most likely applies only to some of the components of the compliance tensor. However, this estimate is qualitatively consistent with the numerical values of D obtained from the property charts in Figure 3.

It should be emphasized that all considerations in this article are not limited to triangular lattices and are applicable to any 2D (and also 3D) lattices with unit cells of any shape. For example, a 3D mesocell obtained by duplicating an octet in each of the three directions will contain 240 independent rods. As a side remark, we note that such a mesocell will already contain the motif of pentamode metamaterial.^[12,35]

Lattices possessing new structural and functional characteristics can be generated by using such mesocells containing rod and node elements with different characteristics. Not only does this refer to elasticity, but it may also apply for electrical and thermal conductivity and other functional properties. A particular area of applications is the development of metamaterials with auxetic and/or chiral characteristics, see some examples in Figure 5. This figure shows part of the motifs for the mesocell with $n = 75$, for which the Z_{1122} component is positive. This means

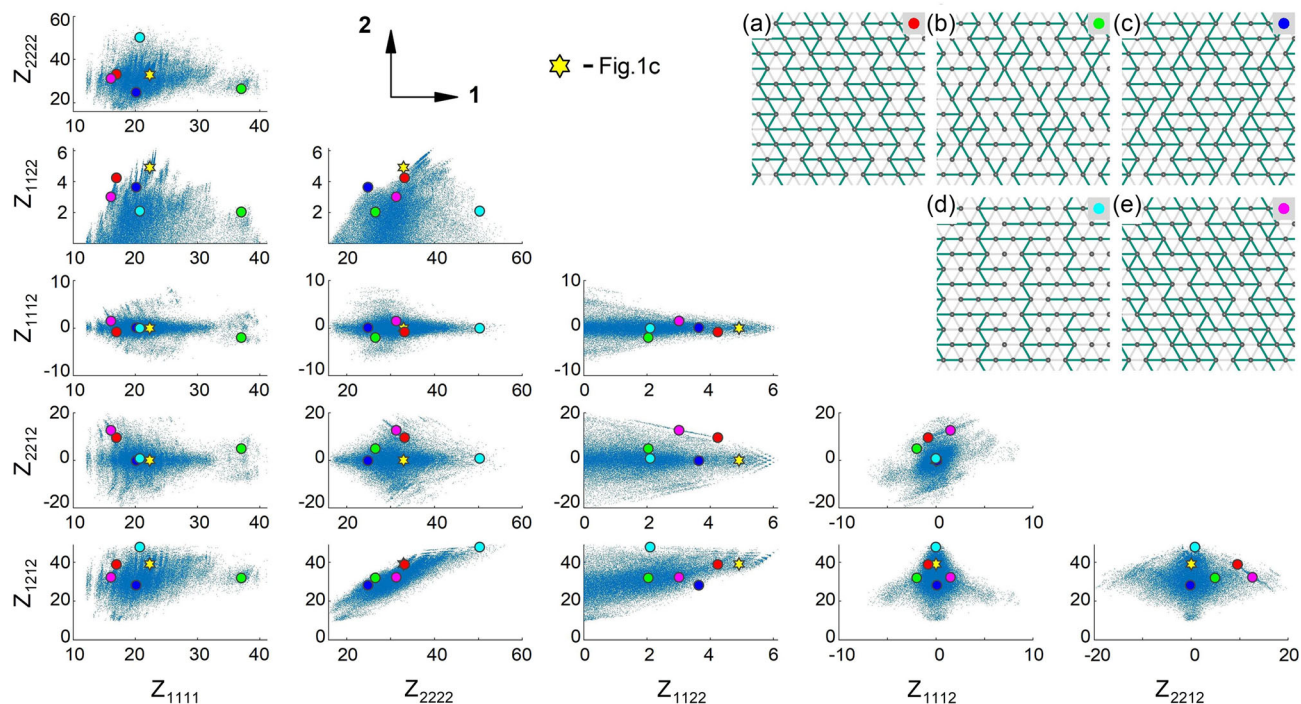


Figure 5. LMMM property charts for auxetics for the mesocell with $n = 75$: a) hard in direction 1; b) soft in direction 1; c) hard in direction 2; d) soft in direction 2; e) a chiral auxetic.

that all these motifs are auxetic. To illustrate the principle of solving the inverse problem, several examples are shown for specific cases when an additional requirement for material properties is introduced.

The LMMM property charts provide a visual representation of the possible range of material properties, which is their important use. In this regard, it is of interest to look at a parallel with the known Hashin–Shtrikman fork described in the context of the composite materials.^[34] It was shown that this “fork” cannot be narrowed if the inner structure of a composite is not considered. In a certain sense, the limit boundary of the LMMM property charts is a multidimensional analog of the Hashin–Shtrikman fork, as it contains the effective moduli of all possible structures. Constraints put on the admissible LMMM structures immediately restrict the property charts making them narrower. This is similar to the narrowing of the Hashin–Shtrikman fork for the property range of a composite by considering its inner structure.

Finally, we note that the LMMM property charts are also useful for solving an inverse problem of finding the material architecture providing desired properties. To that end, the machine learning methods can be employed.^[36–39]

While some of the hypotheses posited in this article require further investigation and substantiation, we believe that it outlines some promising avenues for further research in lattice materials.

6. Conclusion

Our study showed that the rod lattice structures formed by periodic translation of a mesoscale unit cell composed of structural

elements of different types enable a cardinal change of the properties compared with the structures obtained with single-element lattices. This was demonstrated by finite element calculations in conjunction with the Bayesian optimization approach.

2D projections of the multidimensional property space of LMMMs with n structural elements in the mesocell identified by the computations show “demarcation lines” of possible elastic properties of LMMMs on the property charts. The proposed approach enables constructing these charts with a reasonable computational cost.

Calculations showed that for $n > 27$, the growth of the areas of all property charts slows down with increasing n . It was concluded that for $n > 48$, the property chart boundaries are a reasonably good representation of the limit properties of LMMMs with a regular triangular lattice and specified structural elements.

The LMMM property charts provide a guidance to a designer in a quest for materials with desired elastic characteristics and are undoubtedly an important tool for the design of architected lattice materials.

Acknowledgements

This work was performed on the HoreKa supercomputer funded by the Ministry of Science, Research and the Arts Baden-Württemberg and by the Federal Ministry of Education and Research. PG acknowledges the funding support by the Deutsche Forschungsgemeinschaft (DFG, German Research Foundation) under Germany’s Excellence Strategy via the Excellence Cluster 3D Matter Made to Order (EXC-2082–390761711).

Open Access funding enabled and organized by Projekt DEAL.

Conflict of Interest

The authors declare no conflict of interest.

Data Availability Statement

The data that support the findings of this study are available from the corresponding author upon reasonable request.

Keywords

architected materials, Bayesian optimization, elastic anisotropy, lattice metamaterials, machine learning

Received: January 10, 2023

Revised: February 28, 2023

Published online:

-
- [1] M. F. Ashby, *Scr. Mater.* **2013**, *68*, 4.
- [2] Y. Estrin, Y. Bréchet, J. Dunlop, P. Fratzl, *Architected Materials in Nature and Engineering*, Springer Series in Materials Science, Springer Nature, Switzerland AG **2019**.
- [3] Y. Estrin, Y. Beygelzimer, R. Kulagin, P. Gumbsch, P. Fratzl, Y. Zhu, H. Hahn, *Mater. Res. Lett.* **2021**, *9*, 399.
- [4] M. F. Ashby, *Phil. Trans. R. Soc. A* **2006**, *364*, 15.
- [5] N. A. Fleck, V. S. Deshpande, M. F. Ashby, *Proc. R. Soc. A* **2010**, *466*, 2495.
- [6] M. Benedetti, A. du Plessis, R. O. Ritchie, M. Dallago, S. M. J. Razavi, F. Berto, *Mater. Sci. Eng., R* **2021**, *144*, 100606.
- [7] C. Barner-Kowollik, M. Bastmeyer, E. Blasco, G. Delaittre, P. Müller, B. Richter, M. Wegener, *Angew. Chem. Int. Ed.* **2017**, *56*, 15828.
- [8] J. Bauer, L. R. Meza, T. A. Schaedler, R. Schwaiger, X. Zheng, L. Valdevit, *Adv. Mater.* **2017**, *29*, 1701850.
- [9] T. Frenzel, C. Findeisen, M. Kadic, P. Gumbsch, M. Wegener, *Adv. Mater.* **2016**, *28*, 5865.
- [10] P. Ziemke, T. Frenzel, M. Wegener, P. Gumbsch, *Extreme Mech. Lett.* **2019**, *32*, 100553.
- [11] X. Fang, J. Wen, L. Cheng, D. Yu, H. Zhang, P. Gumbsch, *Nat. Mater.* **2022**, *21*, 869.
- [12] J. U. Surjadi, L. Gao, H. Du, X. Li, X. Xiong, N. X. Fang, Y. Lu, *Adv. Eng. Mater.* **2019**, *21*, 1800864.
- [13] K. Liu, R. Sun, C. Daraio, *Science* **2022**, *377*, 975.
- [14] M. Maurizi, C. Gao, F. Berto, *Comput. Mater.* **2022**, *8*, 247.
- [15] R. Zhong, B. Zheng, M. Fu, *Adv. Eng. Mater.* **2021**, *23*, 2000991.
- [16] O. Schwahofer, S. Büttner, J. Binder, D. Colin, K. Drechsler, *Adv. Eng. Mater.* **2022**, 2201385.
- [17] R. Kulagin, Y. Beygelzimer, Y. Estrin, A. Schumilin, P. Gumbsch, *Adv. Eng. Mater.* **2020**, *22*, 2001069.
- [18] M. F. Ashby, *Materials Selection in Mechanical Design*, Butterworth-Heinemann, Elsevier, Oxford **2011**.
- [19] N. Huber, S. R. Kalidindi, B. Klusemann, C. J. Cyron, *Front. Mater.* **2020**, *7*, 51.
- [20] Y. Zhao, N. Schiffmann, A. Koeppel, N. Brandt, E. C. Bucharsky, K. G. Schell, B. Nestler, *Front. Mater.* **2022**, *9*, 821817.
- [21] R. G. Bartle, D. R. Sherbert, *Introduction to Real Analysis*, J. Wiley, New York **2000**.
- [22] A. N. Kolmogorov, *Elements of the Theory of Functions and Functional Analysis*, Dover Publications, Inc., Mineola, NY **1999**.
- [23] L. Mizzi, D. Attard, R. Gatt, K. K. Dudek, B. Ellul, J. N. Grima, *Eng. Comput.* **2021**, *37*, 1765.
- [24] K. Wang, M. Cai, P. Zhou, G. Hu, *Struct. Multidiscip. Optim.* **2021**, *64*, 3911.
- [25] J. Zhou, G. Cui, S. Hu, Z. Zhang, C. Yang, Z. Liu, L. Wang, C. Li, M. Sun, *AI Open* **2020**, *1*, 57.
- [26] K. He, X. Zhang, S. Ren, J. Sun, in *Proc. IEEE Comput. Soc. Conf. Comput. Vis. Pattern Recognit.*, IEEE, Las Vegas, NV **2016**, p. 770, <https://doi.org/10.1109/CVPR.2016.90>.
- [27] Y. Tang, L. Zhang, F. Min, J. He, *IEEE Trans. Ind. Electron.* **2023**, *70*, 2106.
- [28] W. Huang, L. Zhang, H. Wu, F. Min, A. Song, *IEEE Trans. Mob. Comput.* **2021**, <https://doi.org/10.1109/TMC.2022.3174816>.
- [29] W. Huang, L. Zhang, S. Wang, H. Wu, A. Song, *Assoc. Comput. Machin.* **2022**, *22*, 1.
- [30] M. Mirza, S. Osindero (Preprint) arXiv:1411.1784, November **2014**, <https://doi.org/10.48550/arXiv.1411.1784>.
- [31] F. Nogueira, *Bayesian Optimization: Open Source Constrained Global Optimization Tool for Python* **2014**, <https://github.com/fmfn/BayesianOptimization>.
- [32] N. Brandt, L. Griem, C. Herrmann, E. Schoof, G. Tosato, Y. Zhao, P. Zschumme, M. Selzer, *Data Sci. J.* **2021**, *20*, 8.
- [33] R. Kulagin, P. Reiser, K. Truskovskiy, A. Koeppel, Y. Beygelzimer, Y. Estrin, P. Friederich, P. Gumbsch, [Dataset] **2022**, <https://doi.org/10.5281/zenodo.7516301>. <https://kadi4mat.iam-cms.kit.edu/collections/907>.
- [34] M. R. Christensen, *Mechanics of Composite Materials*, Dover Publications, Inc., New York **2012**.
- [35] T. Bückmann, M. Thiel, M. Kadic, R. Schittny, M. Wegener, *Nat. Commun.* **2014**, *5*, 4130.
- [36] Y. Mao, Q. He, X. Zhao, *Sci. Adv.* **2020**, *6*, eaaz4169.
- [37] N. Huber, *Materials* **2021**, *14*, 1822.
- [38] J. K. Wilt, C. Yang, G. X. Gu, *Adv. Eng. Mater.* **2020**, *22*, 1901266.
- [39] J.-H. Bastek, S. Kumar, B. Telgen, R. N. Glaesener, D. M. Kochmann, *PNAS* **2022**, *119*, 1e2111505119.